Supplemental Data for:

Formation of the BMP activity gradient in the *Drosophila* embryo

Claudia Mieko Mizutani†, Qing Nie*[,§], Frederic Y.M. Wan*[,§], Yong-Tao Zhang*[,§], Peter Vilmos[#,£], Rui Sousa-Neves[#,£], Ethan Bier†, J. Lawrence Marsh[#,£,§] and Arthur D. Lander[#,£,§,¥]

†Section of Cell and Developmental Biology,
University of California, San Diego,
La Jolla, CA 92093-0349

*Department of Mathematics, [#]Department of Developmental and Cell Biology, [£]Developmental Biology Center & [§]Center for Complex Biological Systems, University of California, Irvine,
Irvine, CA 92697

1. Effects of varying parameter values

Figure 5 shows the evolution of a gradient of receptor occupancy at a variety of times, and Figure 6 gives profiles of receptor occupancy for particular sets of parameters evaluated at different time points. Figures S1-S6 supplement this information as follows:

Fig. S1 shows the time evolution of the full solution for the parameters in Fig. 5, giving the values for [L], [S], [ST], [T] and [LST] as well as [LR]. The curves depict 5 minute intervals with the final, red curve representing 60 minutes. All gradients start at time=0 from an initial value of zero everywhere.

Fig. S2-S6 show how three characteristics of the dorsal midline peak of [LR] vary when several of the critical parameters are altered, pairwise, over a substantial range from the "base" parameter set of Fig. 5. In each figure, the top left image depicts the peak height at 38 minutes, the time given in Fig. 6. The top right image depicts peak height at 90 minutes. This was used, rather than steady state peak height, because for some parameter sets, steady state occurs later than 90 minutes, a time too long to be biologically significant. The lower left image depicts the time required for the height of the [LR] peak to achieve 63.2% ($1\text{-}e^{-1}$) of its 90-minute value; this

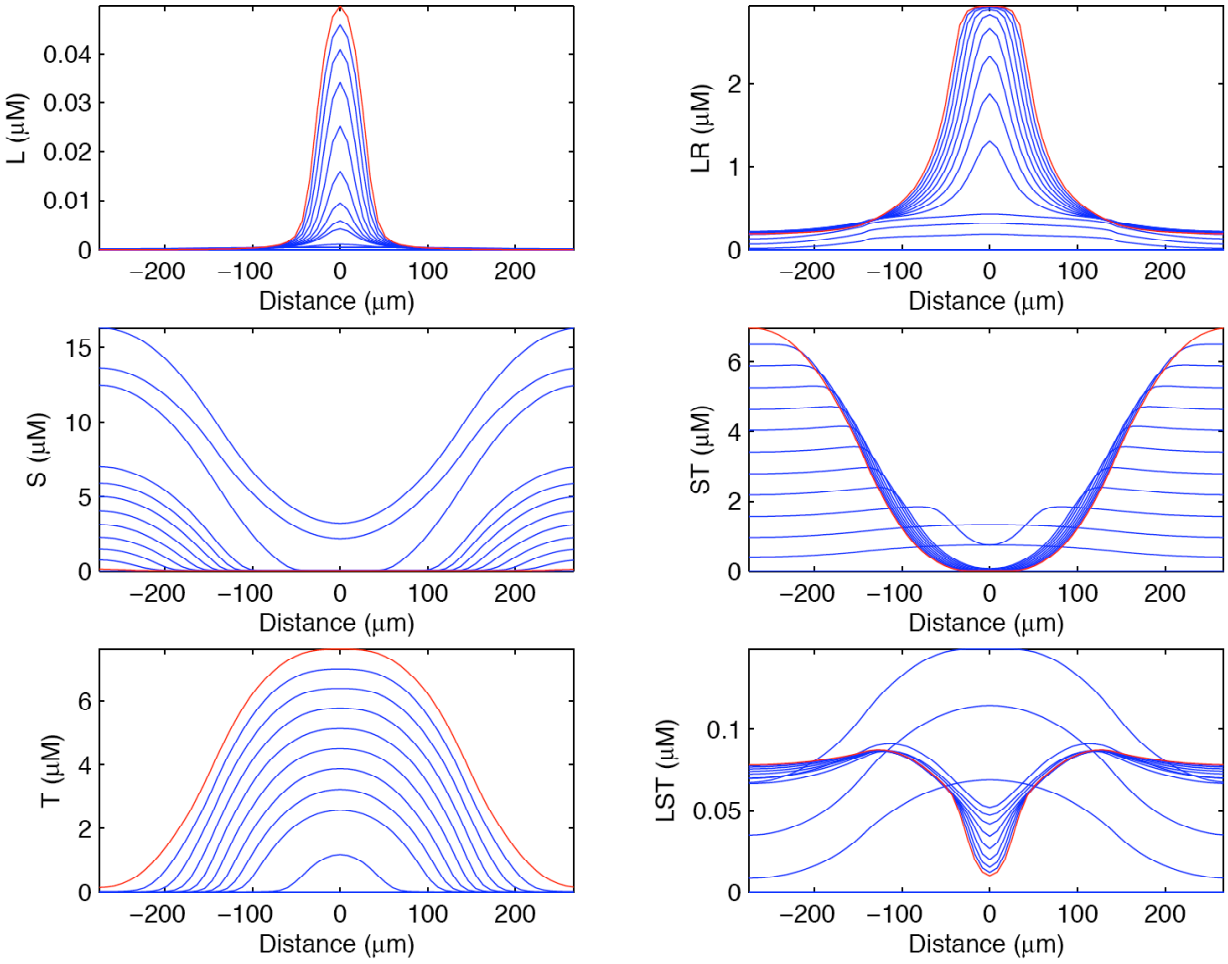

Figure S1. Dynamic behavior of the model, using the parameters in Fig. 5. All concentrations are zero at *t*=0, and correspond to the red curves at t=60 min. The blue curves give values at 5 minute intervals between 0 and 60 minutes.

gives a sense of the overall rate of formation of the BMP activity gradient. The point at the very center of each square represents the parameter set used is Fig. 5.

From Fig. S2-6, one can observe a variety of interesting ways in which the results depend on the parameters. For example, Fig. S2 shows that increasing v_L and v_S have opposite effects on the rate at which the midline signaling peak forms, which helps explain why reducing *sog* gene dosage compensates (under non-steady state conditions) for some of the effect of a reduction in *dpp* dosage (Fig. 7).

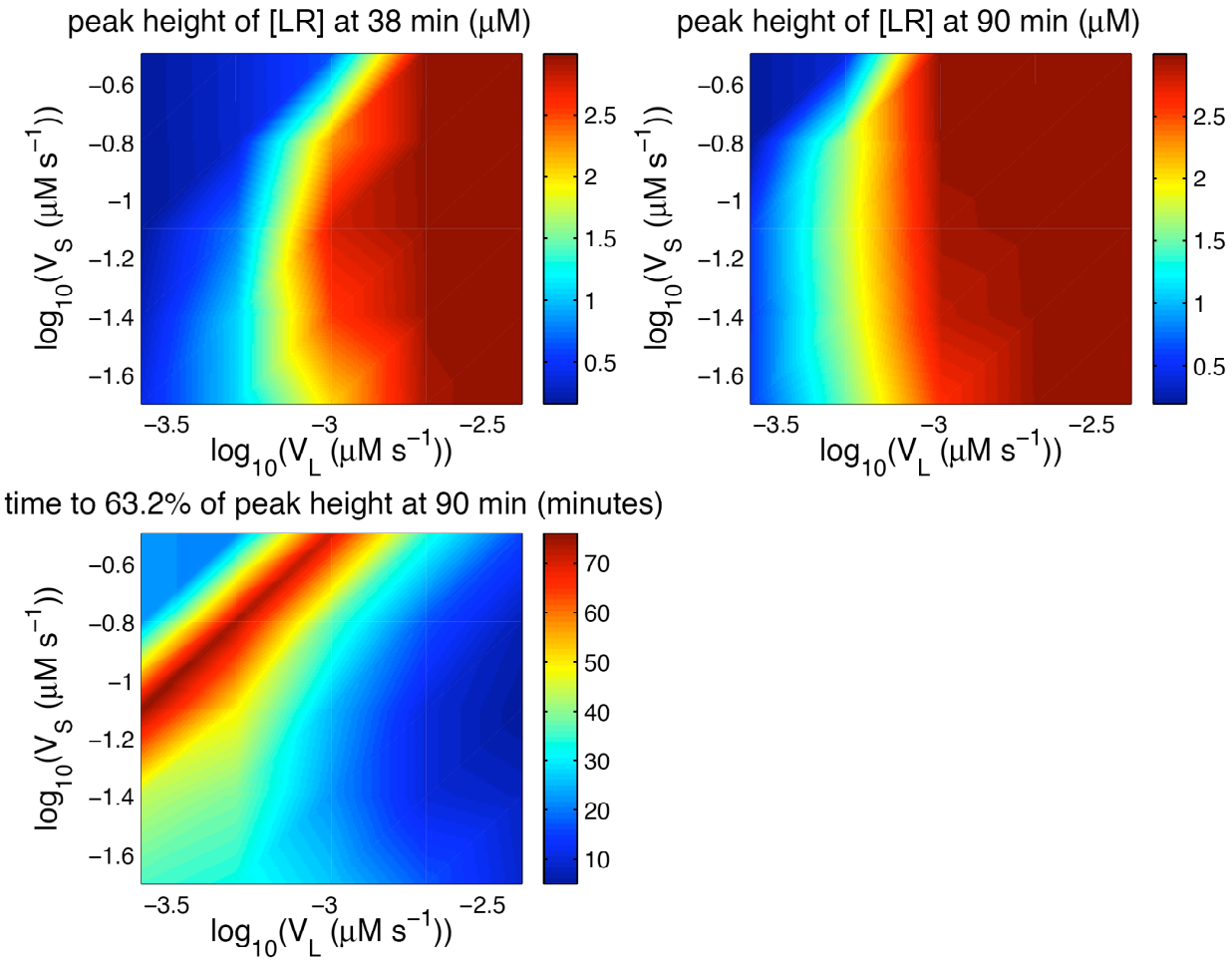

Figure S2. Effect of pairwise variation of v_S and v_L on characteristics of the BMP gradient model of Fig. 4. Top left, value of the dorsal midline peak of [LR] at 38 min. Top right, value of the dorsal midline peak of [LR] at 90 min. Lower left, time for [LR] at the dorsal midline to attain 63.2% of its 90-minute value. The point in the center of each square represents the parameter set used in Fig. 5, and color coding (see calibration bars) is used to represent values of [LR] or time, as appropriate. The model was numerically solved for 25 separate parameter pairs, and contours were generated by interpolation using *Matlab* software.

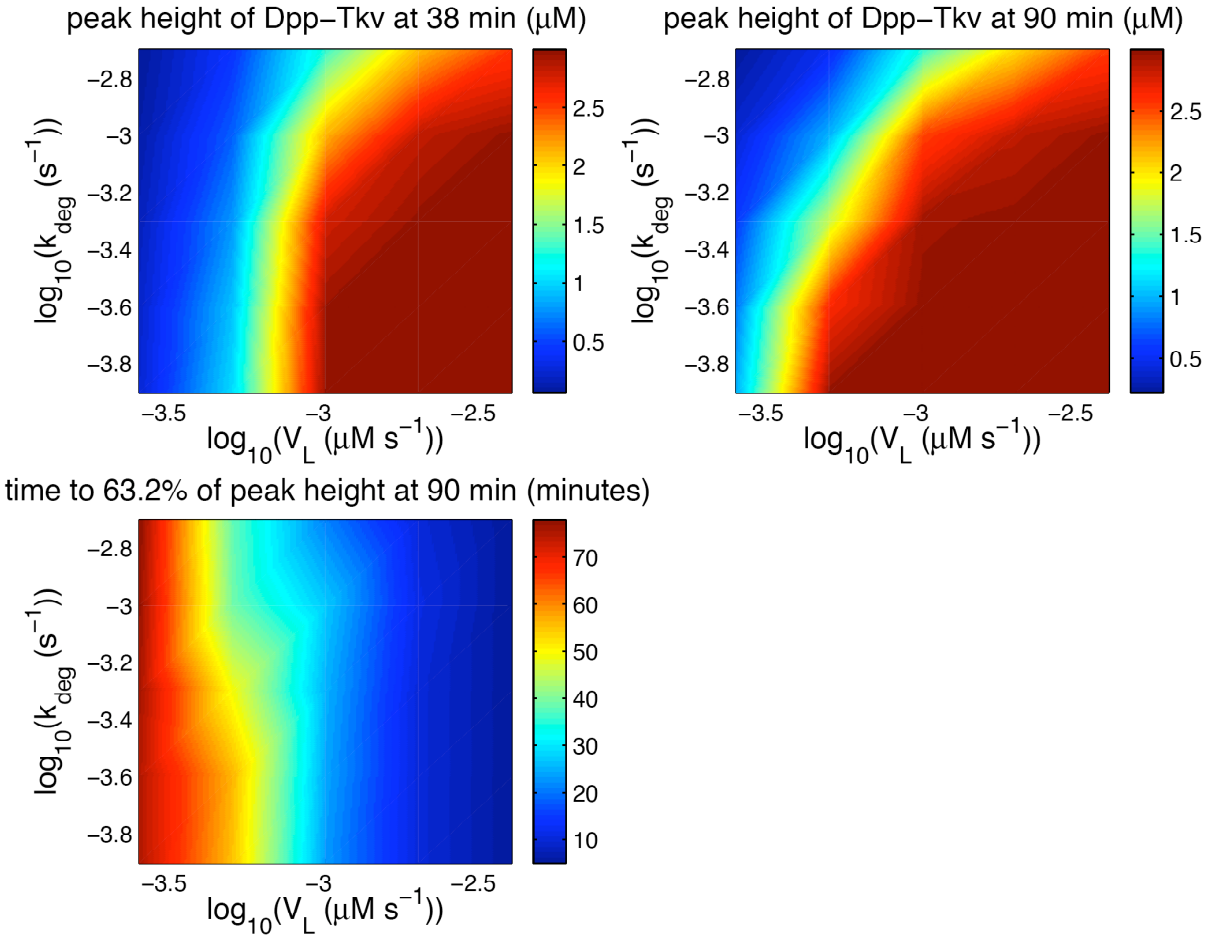

Figure S3. Effect of pairwise variation of k_{deg} and v_L on characteristics of the BMP gradient model of Fig. 4. Top left, value of the dorsal midline peak of [LR] at 38 min. Top right, value of the dorsal midline peak of [LR] at 90 min. Lower left, time for [LR] at the dorsal midline to attain 63.2% of its 90-minute value. The point in the center of each square represents the parameter set used in Fig. 5, and color coding (see calibration bars) is used to represent values of [LR] or time, as appropriate. The model was numerically solved for 25 separate parameter pairs, and contours were generated by interpolation using *Matlab* software.

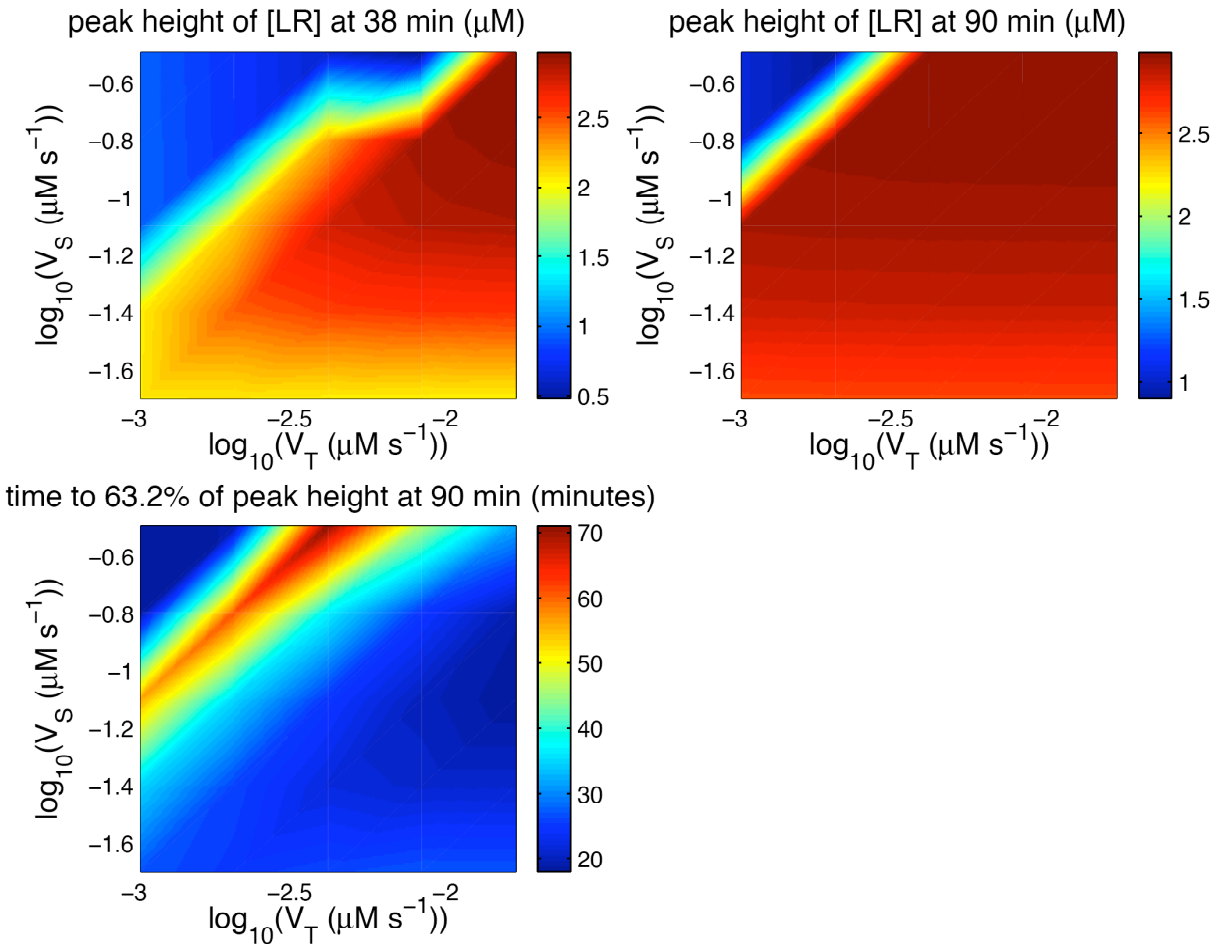

Figure S4. Effect of pairwise variation of v_S and v_T on characteristics of the BMP gradient model of Fig. 4. Top left, value of the dorsal midline peak of [LR] at 38 min. Top right, value of the dorsal midline peak of [LR] at 90 min. Lower left, time for [LR] at the dorsal midline to attain 63.2% of its 90-minute value. The point in the center of each square represents the parameter set used in Fig. 5, and color coding (see calibration bars) is used to represent values of [LR] or time, as appropriate. The model was numerically solved for 25 separate parameter pairs, and contours were generated by interpolation using *Matlab* software.

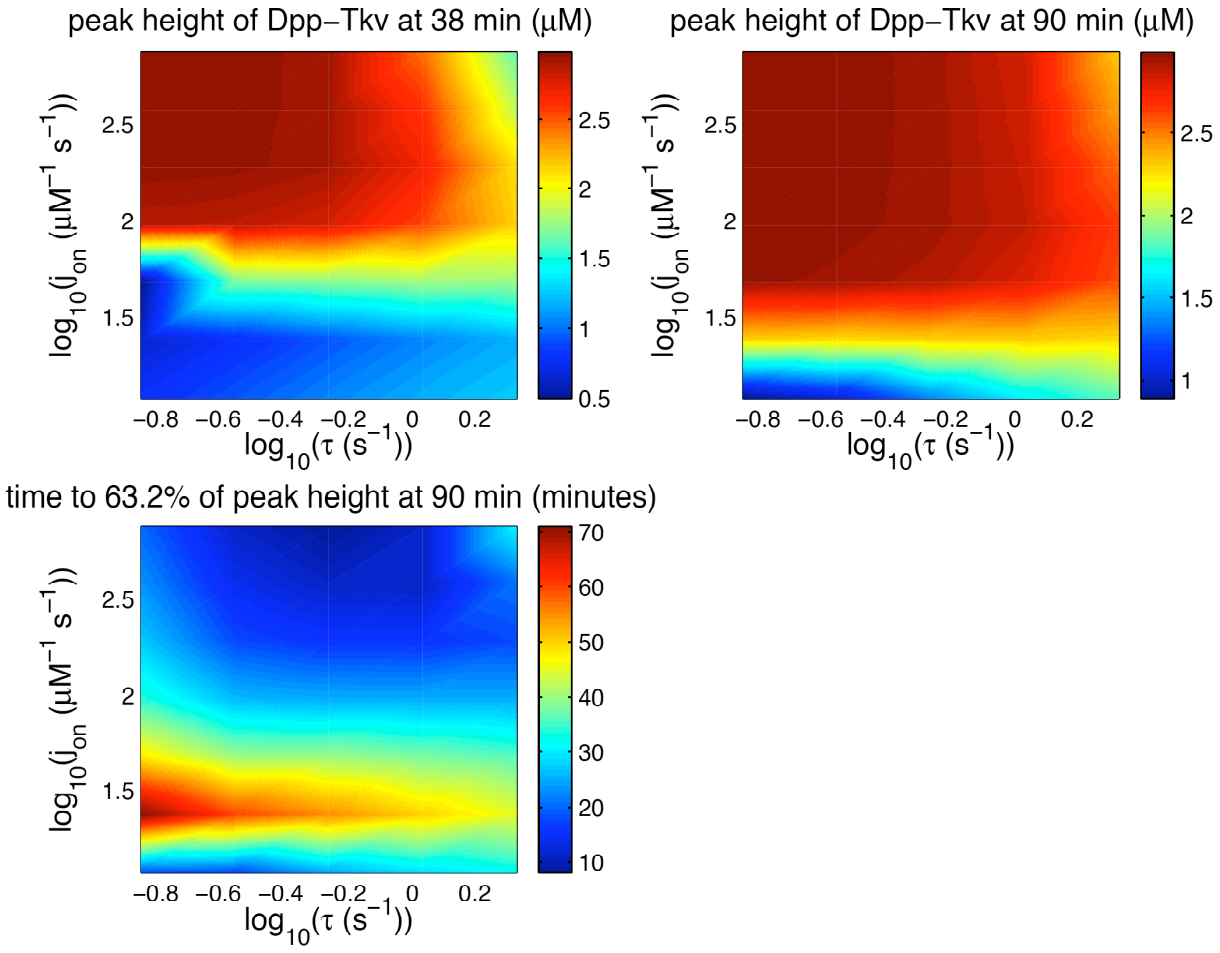

Figure S5. Effect of pairwise variation of j_{on} and τ on characteristics of the BMP gradient model of Fig. 4. Top left, value of the dorsal midline peak of [LR] at 38 min. Top right, value of the dorsal midline peak of [LR] at 90 min. Lower left, time for [LR] at the dorsal midline to attain 63.2% of its 90-minute value. The point in the center of each square represents the parameter set used in Fig. 5, and color coding (see calibration bars) is used to represent values of [LR] or time, as appropriate. The model was numerically solved for 35 separate parameter pairs, and contours were generated by interpolation using *Matlab* software.

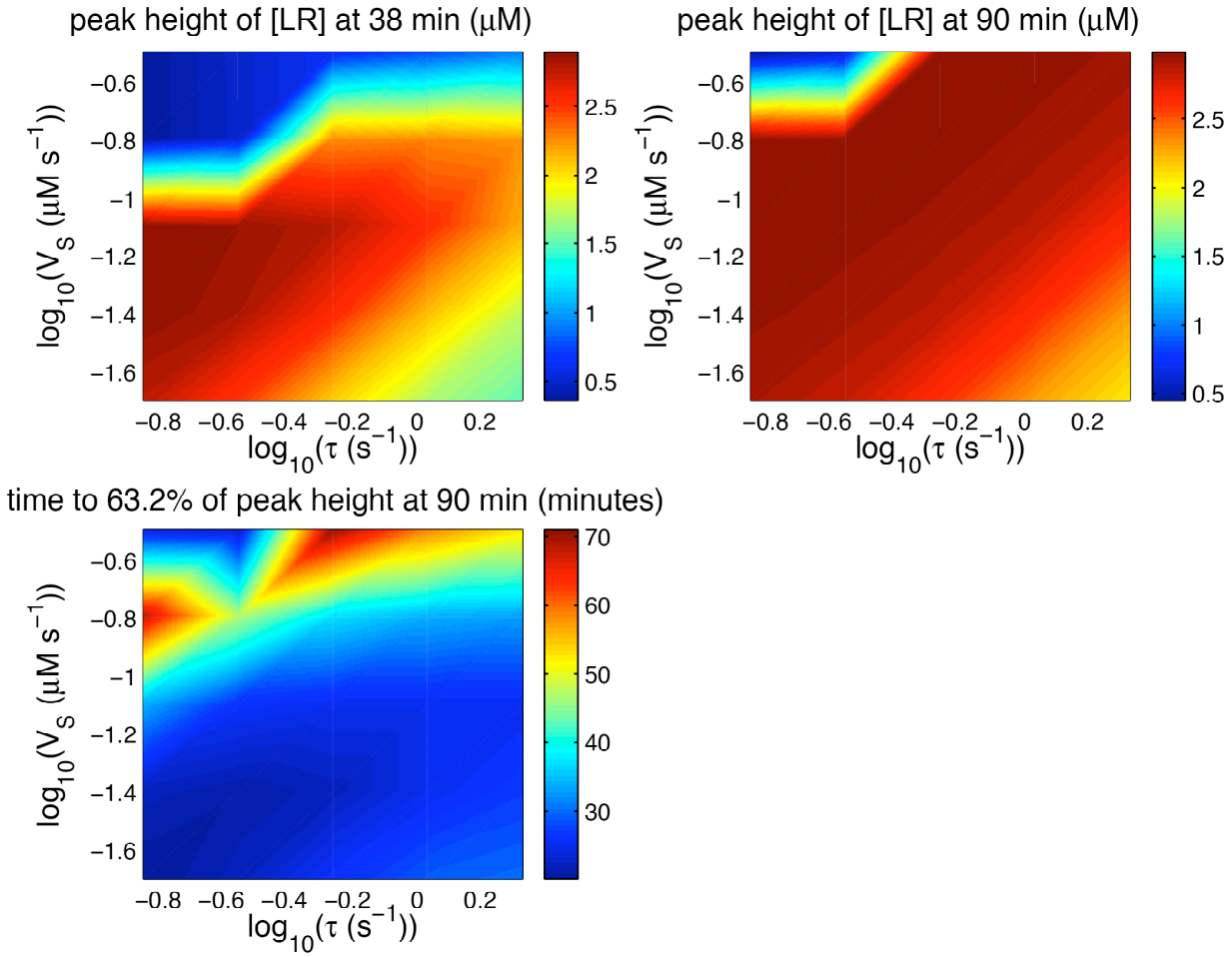

Figure S6. Effect of pairwise variation of ν_S and τ on characteristics of the BMP gradient model of Fig. 4. Top left, value of the dorsal midline peak of [LR] at 38 min. Top right, value of the dorsal midline peak of [LR] at 90 min. Lower left, time for [LR] at the dorsal midline to attain 63.2% of its 90-minute value. The point in the center of each square represents the parameter set used in Fig. 5, and color coding (see calibration bars) is used to represent values of [LR] or time, as appropriate. The model was numerically solved for 25 separate parameter pairs, and contours were generated by interpolation using *Matlab* software.

2. Model structure and parameter choices

We sought to minimize the assumptions and simplifications that went into the reaction diffusion model (Fig. 4) that was studied here. However, in searching for the fundamental behaviors of a system, well-chosen simplifications have practical benefits (e.g. in reducing the size of the parameter space to be explored). Here we point out assumptions and simplifications of the present study.

First, we note that, for our initial conditions (i.e. at time=0) the levels of L, S, T, and their molecular complexes were taken to be zero. In the absence of biological data to suggest otherwise, this is a reasonable choice, but it should be kept in mind that only the steady state solution lacks dependence on the initial conditions. Determining how nonzero initial conditions would alter the time dependent solutions would require more extensive numerical simulations.

Second, we note that Tld was not modeled explicitly, but rather represented by a first order rate constant. This is equivalent to assuming a constant level of Tld at all times and in all locations (in the embryo Tld is produced on the dorsal side and little is known about its protein levels). In the course of initial simulations in which Tld was explicitly modeled (as a dorsally-expressed enzyme that transiently interacts with its substrates), we realized that, due to unhindered diffusion, Tld localization rapidly equilibrated across the embryo. Furthermore, its levels simply increased monotonically with time. It seemed more likely that some degradation process would ultimately slow the rate of Tld increase, but no biological data are available regarding this. It seemed that neglecting such a process (or modeling it with an arbitrarily chosen rate constant) would be just as likely to introduce error as taking Tld levels to be constant, so we took the latter approach.

Similarly, little is known about degradative processes that might counteract a steady rise in the concentration of Tsg due to its continuous production. However, because of its interaction with Sog, we chose to model Tsg explicitly, including its localized production (we note, however, biological data indicating that the location of Tsg expression appears not to be important to patterning [Mason et al., 1997]).

In the case of Sog, Tld-mediated destruction itself counteracts continuous production, so there is no compelling need, from the modeling standpoint, to include other means of removing Sog (and therefore none was included in this study). However, recent experimental data have

demonstrated a Tld-independent, endocytosis-dependent, process of Sog degradation in the embryo (Srinivasan et al., 2002). Thus, we also carried out a series of calculations in which a fixed rate constant of degradation of free Sog was included. While the effects of this change were not tested over as wide a set of parameters as those shown in Fig. S2-S6, we did not observe a dramatic alteration in the general behavior of the system, and found that results similar to those in Fig 5-7 and S1 could be obtained by adjusting the values of other parameters.

It should also be noted that, in the present study we equate [LR] with the morphogen "signal", i.e. PMad. This assumes that PMad is generated rapidly in response to receptor occupancy, and that, when receptor occupancy falls, PMad staining falls as rapidly. We have explored the effects of explicitly defining a "signal" that integrates [LR] over a particular time period, and find that this change has little effect on the results, as long as the rate constant of PMad degradation is reasonably fast.

Finally, we mention that parameter choices were, whenever possible, chosen to fit available experimental data. Choices for the circumference of the embryo, *D* and *R0* follow reasoning similar to that presented by Eldar et al. (2002), although given the sizes of the cells in the embryo, we chose a somewhat higher level of receptors per cell; choices for k_{on} and k_{off} follow references and discussion in Lander et al., (2002). The value of k_{deg} was chosen based on information inferred from Fig. 3 (see text). All other parameters were chosen from within ranges that were consistent with the biophysics of protein-protein interactions and, where applicable, that gave plausible equilibrium binding constants.

3. In vivo effects of receptor overexpression

In the model, receptor-mediated BMP degradation plays an important role in allowing for the formation of relatively stable PMad patterns. To the extent that receptors act as a "sink" for BMPs, one would predict that the localized expression of ectopic receptors would cause a net flux of free BMPs toward the site of receptor overexpression. One result of this would be a depression of BMP signaling in adjacent areas. Recently, Wang and Ferguson (2005) presented experiments in which mRNA for the Dpp receptor Tkv was injected in a localized fashion into early embryos. No discernable differences were observed in the PMad patterns that ultimately

developed, unless a constitutively active form of the receptor was used (a result that was taken in evidence of a signaling-mediated feedback loop that regulates gradient formation).

At first glance, the lack of effect of wild type *tkv* in these experiments would seem to argue against a model in which receptor-mediated BMP degradation is a key event. However, because the experiments of Wang and Ferguson (2005) were carried out by RNA injection, it is not possible to know whether the levels of ectopic *tkv* were substantial compared with endogenous *tkv*, and therefore whether they should have been expected to have any significant influence on BMP degradation. To resolve this issue, we utilized the GAL4-UAS system to express ectopic *tkv* in the head region of embryos, and observed its subsequent effects on PMad staining.

As shown in Figure S7, endogenous *tkv* expression in the embryonic head region is already relatively substantial, and can be elevated by expression of wild type *tkv* using a *bcd*-GAL4 driver. When compared with wild type embryos, those expressing ectopic *tkv* consistently showed a narrowing and weakening of the PMad staining pattern over a range of 10-12 cell diameters posterior to the border of the *bcd* domain. Thus, the data are consistent with the prediction of the model that receptors act as a major BMP sink.

4. A space-independent version of the model

To develop insights into dynamic behaviors of the model that might be independent of morphogen transport, we considered the following additional simplifications: First, we assumed that all molecules were produced everywhere, so that diffusion could be neglected. Second, realizing that in many instances either Tsg or Sog synthesis would be rate limiting for the production of the heterodimeric inhibitor (ST), we represented ST by a single inhibitor species (which for simplicity we refer to as S) that is generated at a constant rate (v_S). Third, we limited our analysis to situations in which receptor occupancy is low enough that levels of free receptors are not appreciably reduced by ligand binding. Fourth, we assume that the rate of dissociation of BMPs from their receptors is slow compared with the rate at which ligand receptor complexes are degraded. With these simplifications, the equations in Fig. 4 can be reduced to the following ordinary differential equations:

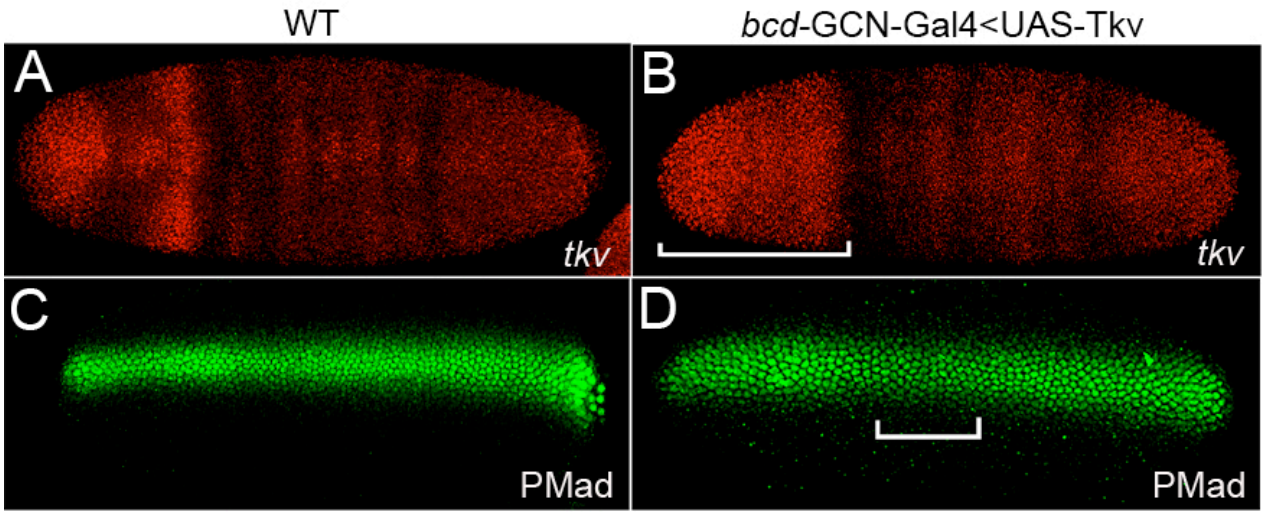

Figure S7. Localized expression of Tkv leads to reduced PMad activation in adjacent cells. A) Endogenous *tkv* expression in a wild-type embryo. Note that expression is elevated in the sections of head relative to the trunk region. At this stage, *tkv* expression is restricted to the dorsal region of the embryo. Embryos are viewed from a dorsal perspective with anterior to the left in this and subsequent panels. B) Over-expression of a UAS-*tkv* transgene in the head with the *bcd*-GCN4/GAL4 driver results in increased *tkv* expression in an anterior cone of cells that circumnavigates the entire D/V axis in the head region (bracket). The level of ectopic *tkv* expression in dorsal cells is approximately equal to that of endogenous *tkv*. C) PMad staining in a wild-type embryo. D) PMad staining in an embryo expressing *tkv* in the head under the control of the *bcd*-GCN4/GAL4 driver. Note that the width and level of PMad expression is decreased in trunk cells lying posterior to the domain of *tkv* over-expression. This depression of PMad staining extends for 10-12 cells (bracket) in which endogenous levels of *tkv* are relatively low at this time (see panel A).

$$\frac{d[L]}{dt} = v_L - k_{on}R_0[L] - j_{on}[L][S] + (j_{off}+\tau)[LS] \quad (1)$$

$$\frac{d[LR]}{dt} = k_{on}R_0[L] - k_{deg}[LR] \quad (2)$$

$$\frac{d[S]}{dt} = v_S - j_{on}[L][S] + j_{off}[LS] \quad (3)$$

$$\frac{d[LS]}{dt} = j_{on}[L][S] - (j_{off}+\tau)[LS] \quad (4)$$

The steady state solutions to these equations are

$$[L]_{ss} = \frac{v_L}{k_{on}R_0}; \quad [LR]_{ss} = \frac{v_L}{k_{deg}}; \quad [S]_{ss} = \left(1+\frac{j_{off}}{\tau}\right)\left(\frac{v_S k_{on}R_0}{v_L j_{on}}\right); \quad \text{and } [LS]_{ss} = \frac{v_S}{\tau}$$

For $v_S > v_L$, we frequently see that the behavior of this system, as elucidated through asymptotic analysis and numerical simulations, can be divided into three phases (Fig S8). During an initial

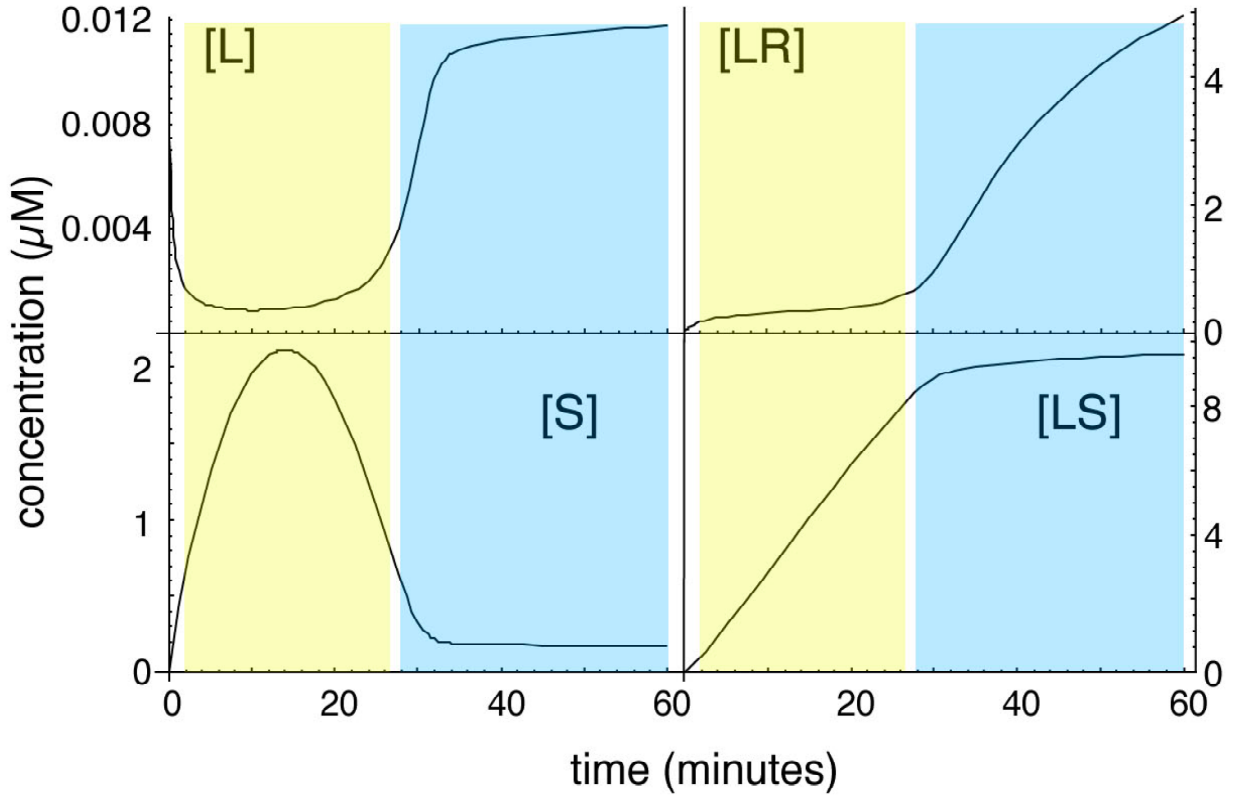

Figure S8. Dynamic behavior of a simplified space-independent model. Equations 1-4 were solved numerically from 0 to 3600 seconds (1 hour). [L], [LR], [S] and [LS] are plotted in units of μM. Parameters were v_L=6 nM; v_S=10 nM; $k_{on}R_0$ = 0.5 sec^{-1}; k_{deg}=0.001 sec^{-1}; $j_{on}R_0$ = 5 sec^{-1}; j_{off}=3x10^{-4} sec^{-1}; τ=0.001 sec^{-1}. Note the distinct "plateau" and "jump" phases, which are shaded in yellow and blue, respectively.

very fast phase, [L] undergoes a rapid rise and fall. For reasonable parameter choices this occurs too quickly to be of biological significance. During a second "plateau phase", [L] and [LR] remain relatively constant, well below their steady state values, [S] rises and then falls, and [LS] rises almost linearly.

The plateau phase ends when [S] falls to near its steady state value. In the subsequent "jump" phase, [L] and [LR] rise rapidly to their steady state values (in some cases undergoing a damped oscillation as they approach those values), while [S] and [LS] remain relatively constant.

This "plateau"-"jump" behavior bears striking resemblance to the behavior of the full system (e.g. Fig. 4) at the dorsal midline (Figure S9; Fig. 5). Therefore, we decided to see how this

behavior, in particular the duration of the plateau phase, depends upon the parameters.

Since simulations show the rise and fall of [S] during the plateau phase is invariably nearly symmetrical, we may estimate the duration of the plateau phase to be twice T, the time for [S] to achieve a maximum, which occurs when $\frac{d[S]}{dt} = 0$. Since, [L] and [LR] are relatively constant during the plateau phase, we may also consider that, at time T, $\frac{d[L]}{dt} \approx 0$. Thus, combining equations 1 and 3 we get that

$$v_L - k_{on}R_0[L]_T - j_{on}[L]_T[S]_T + (j_{off}+\tau)[LS]_T = v_S - j_{on}[L]_T[S]_T + j_{off}[LS]_T$$

where the subscripts indicate evaluation at time T. From this we derive that $[LS]_T = \frac{v_S - v_L + k_{on}R_0[L]_T}{\tau}$. We note that if [L] is well below its steady state value during the plateau phase, then from the steady state solution, we may infer that $k_{on}R_0[L]_T << v_L$. Accordingly, we may approximate

$$[LS]_T = \frac{v_S - v_L}{\tau}. \qquad (5)$$

Combining equations 3-4, we find that $\frac{d[S]}{dt} + \frac{d[LS]}{dt} = v_S - \tau[LS]$. At times close to T, $\frac{d[S]}{dt}$ will be close to zero, and so may be neglected. If we then replace [LS] with its previously estimated value at T from (5), we get $\frac{d[LS]}{dt} \sim v_L$, which agrees with the observed linear rise in [LS] during the plateau phase. Noting that [LS] appears to grow linearly from almost the earliest times, it is appropriate to use the initial condition $[LS]_{t=0} = 0$ in integrating this expression, which gives:

$$[LS] = tv_L, \qquad (6)$$

By requiring equations (5) and (6) both to hold at t=T, we derive that

$$T = \frac{v_S - v_L}{\tau v_L} = \left(\frac{1}{\tau}\right)\left(\frac{v_S}{v_L} - 1\right) \qquad (7)$$

Thus, the duration of the plateau phase, which should be twice the value of T, should vary inversely with τ and, when v_S is large compared with v_L, directly with the ratio $\frac{v_S}{v_L}$. Numerical solutions of the simplified system support this conclusion. Moreover, when the full system (i.e. Fig. 4) is analyzed, one can easily see the same linear dependence of T on $\frac{v_S}{v_L}$ (Figure S10a). Interestingly, the dependence on $\frac{1}{\tau}$ appears to be less than linear (Figure S10b), suggesting that spatial effects that depend upon τ also have an important influence on the full system's behavior.

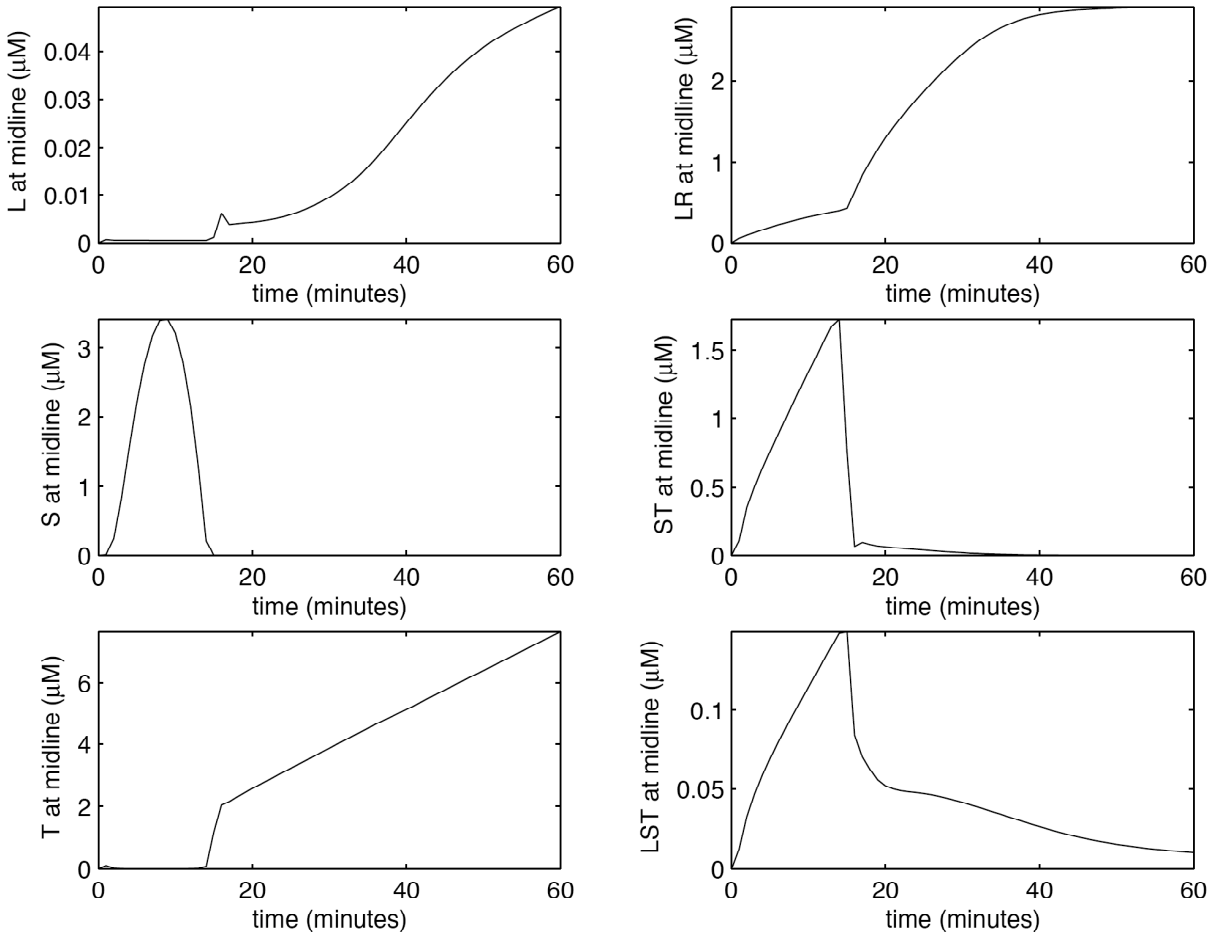

Figure S9. Dynamic behavior of the full model at the dorsal midline. The equations in Fig. 4 were solved for the parameters listed in Fig. 5. Values of [L], [LR], [S], [ST], [T], and [LST] at the dorsal midline (x=0) are plotted as a function of time. Note the distinct "plateau" and "jump" phases of the [L] and [LR] curves. As in the space-independent model (Fig. S8), the plateau phase is characterized by a nearly symmetrical rise and fall in [S], and a nearly linear rise in [LST].

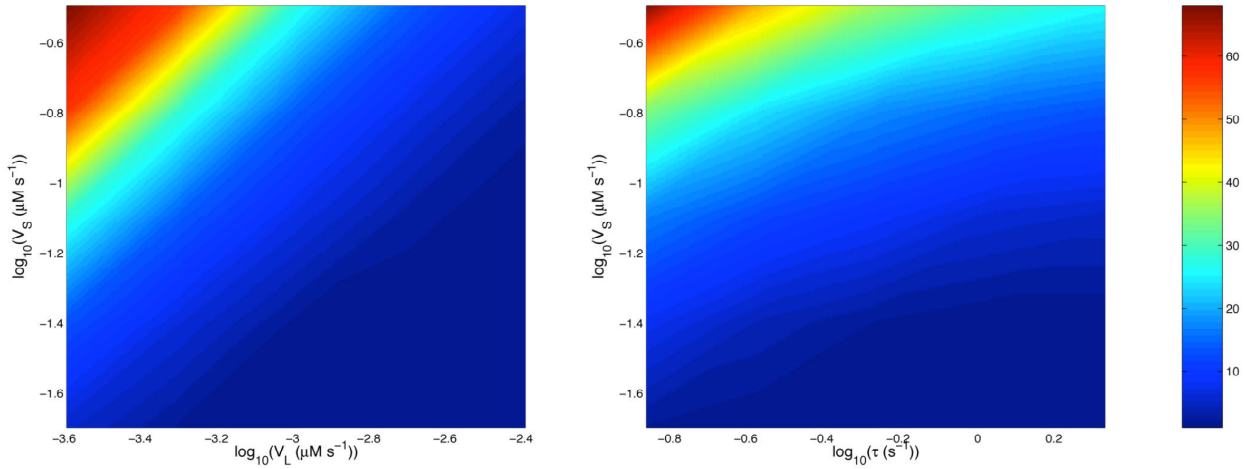

Figure S10. Time for [S] to reach a maximum at the dorsal midline, as a function of v_L and v_S (left image) or τ and v_S (right image), for the complete model shown in Fig. 4. To create each image, the model was numerically solved for 25 separate parameter pairs, and contours were generated by interpolation using *Matlab* software. Time (in minutes) is represented by color coding (see calibration bar). Parameters corresponding to those used in Fig. 5 are located at the center of each square. In the left image, the contour lines all exhibit a slope=1, indicating that the time for [S] to reach a maximum at the dorsal midline is directly proportional to v_L/v_S. In the right image, the lower slope of the contour lines indicates that the time for maximum [S] is less sensitive to τ than predicted.

5. Effect of expression level on range of morphogen action

According to Fick's law, the flux of a diffusing species will be proportional to its concentration gradient. Accordingly, even if a molecule has low intrinsic diffusivity, there can be a substantial flux of it away from a source if the concentration gradient is large enough. Thus, with a high enough level of production, a morphogen should be able to act at a substantial distance even if its diffusivity is very low. In the experiments in Fig. 2-3, st2-*dpp* is expressed at a level up to 2.5 times higher than endogenous Dpp. We wished to address whether this amount of overexpression could have had a significant effect on the observed range of action, leading Fig. 2-3 to overestimate the range that endogenous Dpp would normally have in the absence of Sog.

In a *sog*- embryo expressing st2-*dpp*, we may model morphogen gradient formation as a one-dimensional problem (particularly if endogenous Dpp is ignored or, even better, eliminated genetically as in Fig. 3): Morphogen is produced at rate v_L in a zone of width "*p*" equal to the width of *eve* stripe 2, and diffuses out in anterior and posterior directions, with diffusivity *D*. Receptors are assumed to be uniformly distributed, and to bind and degrade morphogen with rate

constant k_{deg}. We have analyzed this problem elsewhere (Lander et al., 2002; Lander et al., 2005) and may obtain approximate steady state solutions in two regimes:

When v_L is sufficiently low that levels of morphogen are nowhere high enough to saturate the majority of receptors, the gradient of receptor occupancy [LR], as a function of distance x from either edge of the morphogen production region, is approximated by exponential decay:

$$[\mathrm{LR}] = \frac{v_L}{k_{deg}} \frac{e^{-x\Lambda}}{1+coth(\Lambda\frac{p}{2})} \tag{8}$$

In this formula, the production region is given by $-p<x<0$, and the gradient region on one side of the production region by $x>0$. The parameter Λ is a length constant (units of length^{-1}) given by

$$\Lambda = \sqrt{\frac{k_{deg}k_{on}R_0}{D(k_{off}+k_{deg})}},$$

where k_{on}, k_{off} and R_0 have their usual meanings (Lander et al., 2005). The inverse of Λ is roughly equivalent to what Eldar et al. (2003) call the degradation length.

Diffusivity enters into the formula in (8) through the fact that Λ is inversely proportional to the square root of D. Decreasing D thus increases Λ and makes the exponential term in the numerator fall more rapidly. It also lowers the value of LR at the start of the gradient (i.e. $x=0$) by decreasing the value of $1+coth(\Lambda\frac{p}{2})$, although it should be noted that once $\Lambda\frac{p}{2}\geq 1$, the effect of varying Λ on this term is small.

Using the parameters given in the legend to Fig. 5, and an approximate width for *eve*-st2 of 35μm, we get $[\mathrm{LR}] \approx 0.98e^{-0.12x}$, which describes a morphogen gradient that falls from 33% to 0.33% receptor occupancy over about 39 μm. This is on the order of size of the signaling gradient we observe in Fig. 3. In contrast, were we to use a value of D 100-fold lower than that of a freely diffusible protein, we would have $[\mathrm{LR}] \approx e^{-1.2x}$, which falls from 33% to 0.33% receptor occupancy over 3.9 μm. This is much smaller than the signaling gradient observed in Fig. 3. However, by adjusting the parameters, we might be able to boost this value. According to equation 8, there are three ways we might do this: (1) We could increase v_L, so that more ligand is made, and the gradient therefore starts from a higher level of receptor occupancy. (2) We could modify some of the parameters that determine the value of Λ to directly counteract the effects of lowering D. (3) We could assume that cells detect even very low levels of receptor

occupancy (for example, when receptor occupancy may be 0.33% at 3.9 μm, if cells were able to detect 0.00033% receptor occupancy then signaling could extend to almost 10 μm.

As it turns out, there are limitations that prevent us from using any of these strategies to great effect. Strategy 1 is limited by the fact that, for sufficiently high v_L, receptor occupancy will approach saturation, and equation 8 will no longer apply (more about how to analyze such cases will be discussed below). Strategy 2 is limited by the fact that, although Λ is a function of several parameters, under conditions of rapid receptor-mediated morphogen degradation, $k_{deg} >> k_{off}$, so that both k_{deg} and k_{off} drop out from the definition of Λ. Since we have specified that D is 100 fold below that of free diffusion, we get $\Lambda = \sqrt{\frac{k_{on}R_0}{0.85\ \mu m^2\ sec^{-1}}}$. However, since our choice of k_{on}=0.4 $\mu M^{-1}sec^{-1}$ is already at the lower limit of what is typically observed for ligand-receptor association rate constants (Lander et al., 2002), we may consider that $\Lambda = \sqrt{0.471R_0}$, and our only option for decreasing Λ is to decrease R_0.

Indeed, it follows from equation 8 that, for x>0, increasing v_L by n-fold will shift values of LR farther from the origin by a distance $\Delta x = \frac{\ln n}{\Lambda} = \frac{\ln n}{\sqrt{0.471R_0}}$. By choosing a value for R_0 that is low enough, it should be possible—in theory—to expand a gradient by any desired Δx, regardless of the value of n. In practice, however, we may not use values of R_0 so low that there are too few receptors per cell to allow generation of a signal. Let R_1 stand for the minimum concentration of receptors that must be occupied for signaling to take place. Let θ_0 stand for the value of [LR] at x=0, normalized to R_0, that results when v_L is increased n-fold from its usual value. Then, by equation 8, $[LR] = \theta_0 R_0 e^{-x\Lambda}$ (for x>0). The distance x at which this expression falls below the threshold for signaling can be found by solving $R_1=\theta_0 R_0 e^{-x\Lambda}$ for x. This yields

$$x = \frac{-1}{\Lambda}\ln\frac{R_1}{\theta_0 R_0} = \frac{-1}{\sqrt{0.471R_0}}\ln\frac{R_1}{\theta_0 R_0}.$$

Any attempt to expand a gradient by more than this distance will be futile, as no signaling can occur past this point. Setting our previous expression for Δx to this value allows us to determine that this will happen when $R_0=\frac{nR_1}{\theta_0}$, and Δx=1.46 ln n $\sqrt{\frac{\theta_0}{nR_1}}$. This expression, then, represents the maximum amount by which a gradient may be extended by increasing v_L and decreasing R_0. Since this results follows from equation 8, it only holds when receptor saturation

is not high, a condition that also constrains $\theta_0 \leq 0.5$.

R_1, the minimum concentration of receptors that must be occupied for signaling to occur must, for obvious reasons, be at least 1 receptor per cell. However, we note that both *race* expression and PMad staining (the signals measured in Fig. 2-3) are relatively high threshold BMP responses, so we must pick a larger value of R_1, lest there be no possibility for low threshold responses. Five receptors per cell would seem to be a very conservative lower limit. Converting units of receptors/cell to molarity requires information about cell size and the volume of the perivitelline space; drawing upon arguments similar to those in Lander et al., (2002) as well as those used by Eldar et al., (2002) we calculate that 5 receptors per cell represents a concentration in the perivitelline space of ≈0.00163 μM.

Using this value for R_1 and 0.5 for θ_0 we get $\Delta x = 25.5 \frac{\ln n}{\sqrt{n}}$. The maximum value this expression can attain is 18.8 μm, which occurs when $n \approx 7.4$ (i.e. an increase in v_L of 7.4 fold). In Figures 2-3, where the increase in v_L was estimated as no more than 2.5 fold, the value of this expression is no more than 14.8 μm, about two cell diameters. This is much less than the observed range of action of ectopic Dpp in the absence of Sog. From this we infer that, had ectopic Dpp been expressed at wild type levels, instead of levels 2.5 fold higher, the resulting gradients of Dpp activity would have still exhibited a considerable range, just a few cell diameters lower than what was observed in Fig. 2-3.

As already mentioned, the previous analysis depends upon the validity of equation 8, which does not apply when v_L is large enough, or R_0 small enough, that receptor saturation is high near the morphogen source. We now turn our attention to such situations. These cases produce receptor occupancy gradients that are sigmoidal in shape, with [LR] being nearly constant ([LR] $\approx R_0$) for some distance away from the morphogen source, and then falling in a manner that ultimately fits an exponential decay curve (Fig. S11a-b). The analysis of this situation is discussed, in part, in Lander et al., 2005, and will be further elaborated elsewhere (Lander, Nie and Wan, in preparation). However, it is relatively straightforward to show that x_C, the critical distance at which such curves fall to 50% receptor occupancy, is approximately equal to $\frac{p}{2}(\beta\text{-}1)$, where $\beta = \frac{v_L}{k_{deg} R_0}$. This can be understood intuitively by noting that, when β=1, morphogen

production at each location within the production region (v_L) exactly equals the maximum rate at which the morphogen can be degraded ($k_{deg}R_0$) at that location. Thus, when $\beta > 1$, morphogen production exceeds the amount that can be destroyed locally by a factor equal to β-1. Given that cells outside the production region degrade the morphogen at the same maximum rate as those within, one would expect that the total distance outside the production region that would be needed to absorb all of the excess morphogen produced in the production region would be the size of the production region times the factor by which morphogen is produced in excess there, i.e. $p(\beta\text{-}1)$. Allocating this distance equally to either side of the production region justifies the formula $x_C = \frac{p}{2}(\beta\text{-}1)$.

From this analysis we see that, in cases in which receptor saturation is high near morphogen sources, we may roughly divide gradients into a highly saturated zone ($0<x<x_C$, receptor occupancy>50%) followed by an exponential decay zone. While the shape of the gradient within the exponential decay zone will certainly depend on D in the manner just described for gradients in which receptors are far from saturation, we note that x_C is independent of D, and increases monotonically with v_L. Indeed, for $\beta >> 1$, $x_C \approx \frac{p}{2}\beta$, so the width of the highly saturated zone should expand nearly linearly with v_L. Simulations confirm that this is the case (Fig. S11c).

Figure S11 (page following). Behavior of morphogen gradients formed when rates of morphogen synthesis are high enough to saturate receptors close to the morphogen source. To investigate the ability of changing levels of morphogen synthesis to compensate for possible reduced diffusivity of Dpp, the diffusion coefficient used in these calculations was 100 fold below that of a soluble protein. A) Time evolution of gradients generated by four different values of v_L. In each case, the gray area represents the region in which morphogen synthesis takes place, and the number in the upper right gives the value of v_L normalized to $k_{deg}R_0$. The time interval separating the individual blue curves is 10 minutes. B) Steady state values of time evolution curves such as those in panel A, for eight different values of v_L normalized to $k_{deg}R_0$: 0.25, 0.5, 1, 2, 3, 5, 8 and 16. C) Relationship between x_C, the location at which the steady state value of [LR] = 0.5 R_0, and $\beta - 1 = (v_L/k_{deg}R_0) - 1$. The circles represent individual data points calculated from the curves in panel B. The dashed line is the predicted relationship between x_C and β (see text). D) Relationship between β and the time required for the value of [LR] at $x=x_C$ to attain 90% of its steady state value of $0.5R_0$. The parameters used in panels A-D were: $D=0.85\ \mu m^2\ sec^{-1}$; $p=35\ \mu m$; $R_0=0.5$; $k_{on}=0.1\ sec^{-1}$; $k_{off}=10^{-5}\ sec^{-1}$; $k_{deg}=5\ 10^{-4}\ sec^{-1}$.

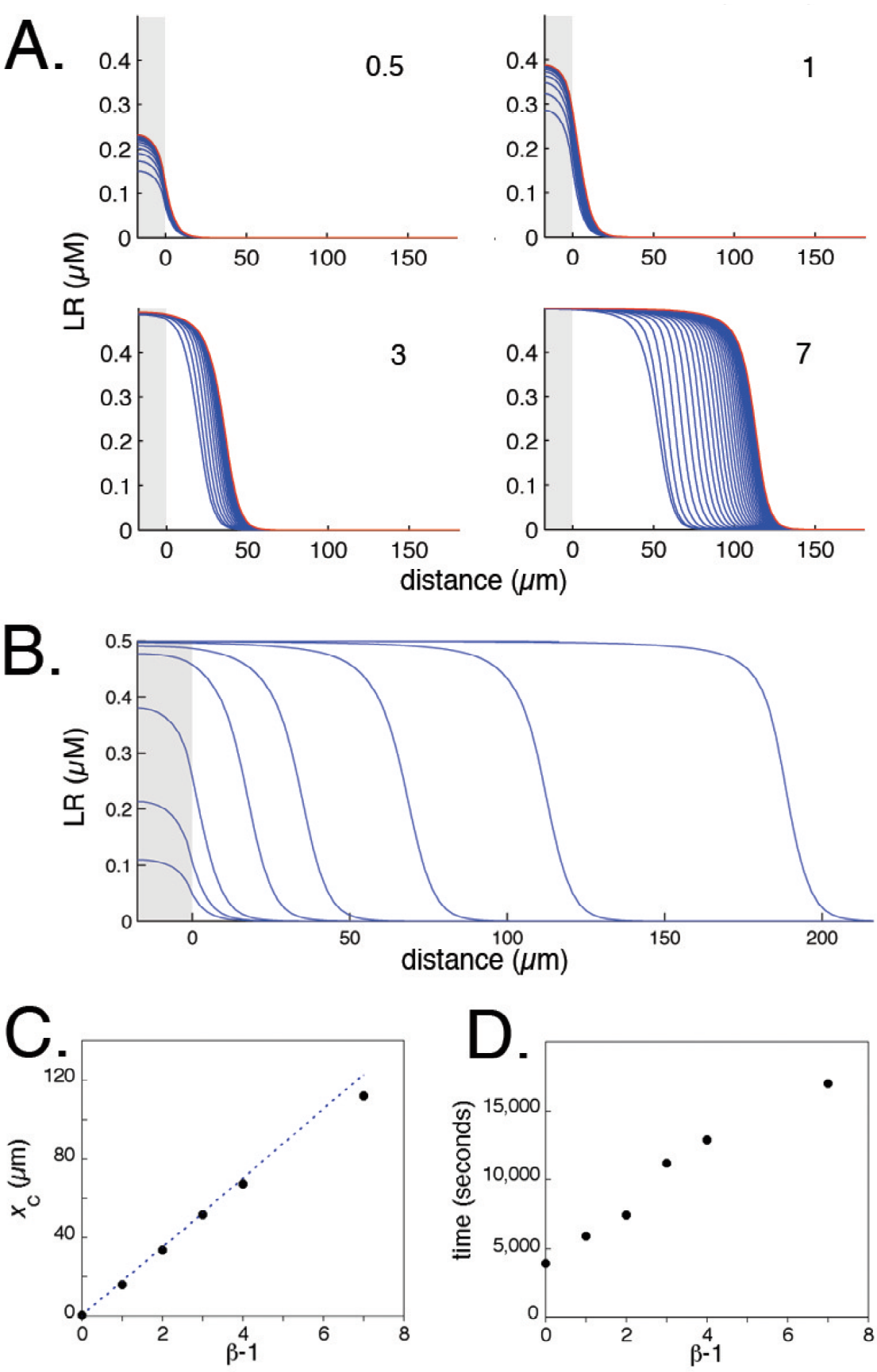
A.
0.5
1
3
7
LR (μM)
distance (μm)
B.
LR (μM)
distance (μm)
C.
x_c (μm)
β-1
D.
time (seconds)
β-1

Given this behavior, overexpression of a morphogen by 2.5 fold could potentially extend its range of action by almost 2.5 fold. However, we can be fairly certain that the condition $\beta>>1$ does not hold when Dpp is produced at its endogenous levels. This is because, in *sog*- embryos, PMad signaling across the dorsal region (where endogenous Dpp is expressed) is considerably lower than the strong PMad signal seen at the dorsal midline of wildtype embryos. Thus, within the broad domain of Dpp production, the wild type rate of Dpp production must be insufficient to saturate all receptors (in agreement with this, the parameter values chosen for Fig. 5 imply $\beta=0.67$). If we increase v_L by 2.5 fold (the amount by which st2-*dpp* expression exceeds that of endogenous *dpp* in Fig. 2), β will be 1.67, putting x_C at 1/3 the width of a st2 domain, or about two cell diameters. As stated in previously, this is small compared with the overall range of action of st2-*dpp* in Fig. 2-3.

Although the above insights were derived from an examination of steady state behavior, further analysis shows that the rate of approach of such gradients to steady state increases for larger v_L (Fig. S11d), further diminishing the ability of increased v_L to cause significant gradient expansion within a reasonable time frame.

In summary, in regimes of either low or high receptor saturation, if Dpp diffusivity is taken to be 100 fold lower than that of a typical soluble protein, overexpressing Dpp to a degree similar to that in Fig. 2-3 should not have been able to expand the Dpp activity gradient significantly. Accordingly, the data do not support very low Dpp diffusivity.

6. Conditions under which soluble inhibitors extend morphogen range of action

In the text we assert that any diffusible inhibitor can extend the range of action of a morphogen, even one that is not subject to ligand-induced destruction. This follows from an analysis of the one-dimensional model of a morphogen gradient, and its approximate solution when receptor occupancy is not close to saturation, i.e. equation 8.

If we assume that a competitive inhibitor of morphogen binding is present in such a system, and at a uniform level everywhere, then some fraction of free morphogen molecules will be bound to inhibitor, and therefore unable to complex with receptors. Accordingly, the rate at

which morphogen molecules bind to receptors will go down by exactly the fraction of morphogen molecules that is complexed with inhibitor. As such, the effect of the inhibitor on the steady state distribution of morphogen-receptor complexes can be seen as equivalent to a decrease in the association rate constant k_{on}. Λ will therefore decrease by the square root of that fraction.

What will the effect of a lower Λ be on the LR gradient? Both the numerator and denominator of equation 8 will increase, suggesting that the overall gradient might either expand or contract, depending upon the parameter values. This is in fact the case. The family of curves in Figure S12 show that as Λ decreases, curves become broader, but also lower. When $\Lambda p >> 2$,

Figure S12. Predicted effect of a diffusible inhibitor on the steady state profile of a morphogen gradient. According to equation 8, if receptor occupancy (i.e. [LR]) is normalized to v_L/k_{deg}, and distance is scaled to the width of the morphogen production region, p, then receptor occupancy versus distance depends only on the unitless parameter Λp. Since Λ is proportional to $\sqrt{k_{on}}$, and the presence of a diffusible inhibitor may be modeled as a decrease in k_{on}, we represent the effect of increasing amounts of inhibitor with a series of curves of decreasing Λp (values of Λp are shown next to each curve). Each twofold decrease in Λp may be thought of as the addition of an amount of soluble inhibitor that lowers by fourfold the amount of free morphogen. Because decreasing Λp makes morphogen gradient profiles both lower and broader, the range of morphogen actions may either increase or decrease, depending on the initial value of Λp and the threshold level of [LR] required by cells for morphogen response.

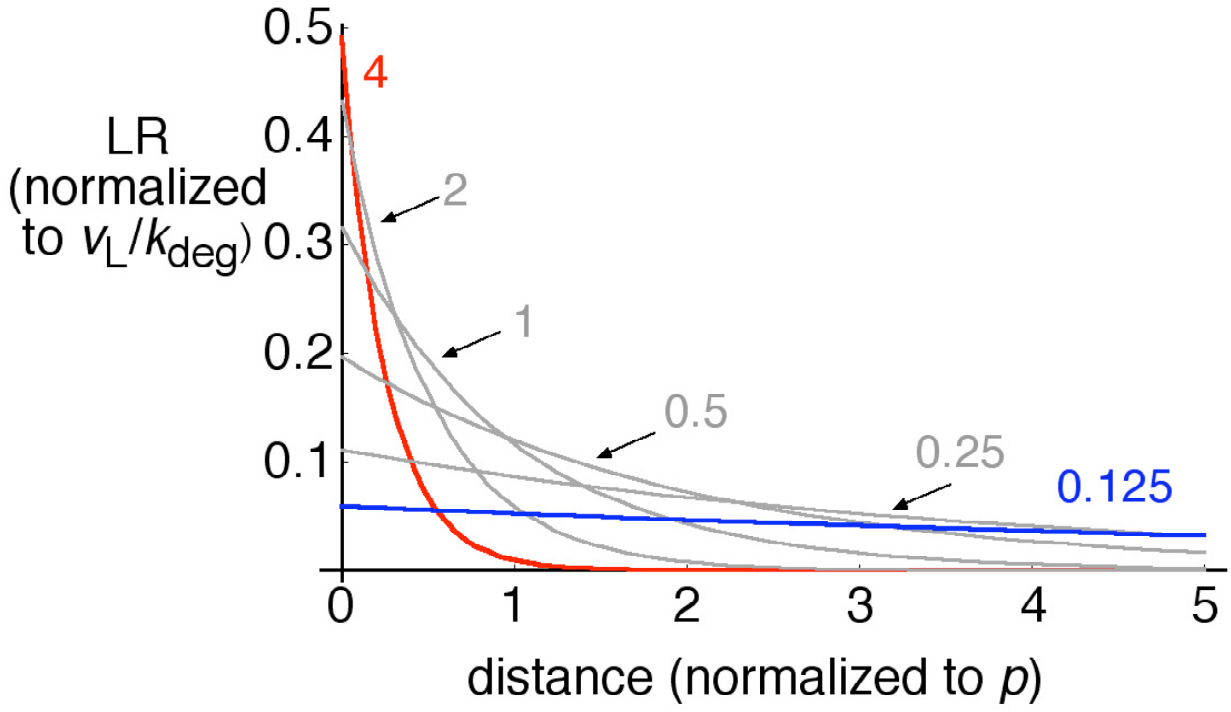

the dominant effect of decreasing Λ is broadening; when $\Lambda p << 2$, the dominant effect is lowering. Since Λ^{-1} specifies the distance over which such a morphogen gradient declines to ~37% of its value at x=0, we may rephrase the preceding statement as follows: As long as the region over which a morphogen gradient is spread does not too greatly exceed the width of the region that produces the morphogen, the addition of a diffusible inhibitor can significantly extend the effective range of most morphogen actions. The qualification, "most" is included in the previous sentence because, as Fig. S12 shows, the amount of range extension depends on the threshold of the morphogen response. For example, when one compares the curves representing Λp=4 with Λp=1, one sees that the width of a cellular domain specified by a morphogen response with a threshold level of 0.2 will expand more than twofold, while a domain specified by a response with a threshold level of 0.3 will contract more than twofold.

Note that, in Fig. 3c-e, the region of morphogen production is clearly on the same order as the width of the Dpp activity gradient. Thus, one would expect the presence of modest amounts of a soluble inhibitor to expand the range of Dpp action for most response thresholds. Whether Sog, at its endogenous levels, is in the optimal range to have such an effect is not known, but from the simulations in Fig. S1 we see (at least when the parameters in Fig. 5 are used) that about 3/4 of the Dpp that is not receptor-bound is complexed with Sog. This would suggest that the inhibitory effects of Sog could be equated with a two-fold decrease in effective Λ, the consequences of which (according to Fig. S12) could be sufficient to explain much of the greater range of Dpp action in *sog*+ vs. *sog*- embryos.

References

Eldar, A., Dorfman, R., Weiss, D., Ashe, H., Shilo, B. Z., and Barkai, N. (2002). Robustness of the BMP morphogen gradient in *Drosophila* embryonic patterning. Nature *419*, 304-308.

Eldar, A., Rosin, D., Shilo, B. Z., and Barkai, N. (2003). Self-enhanced ligand degradation underlies robustness of morphogen gradients. Dev Cell *5*, 635-646.

Lander, A. D., Nie, Q., and Wan, F. Y. (2002). Do morphogen gradients arise by diffusion? Dev Cell *2*, 785-796.

Lander, A. D., Nie, Q., and Wan, F. Y. M. (2005). Spatially distributed morphogen synthesis and morphogen gradient formation. Math Biosci & Eng *In press*.

Mason, E. D., Williams, S., Grotendorst, G. R., and Marsh, J. L. (1997). Combinatorial signaling by Twisted Gastrulation and Decapentaplegic. Mech Dev *64*, 61-75.

Srinivasan, S., Rashka, K. E., and Bier, E. (2002). Creation of a Sog morphogen gradient in the Drosophila embryo. Dev Cell *2*, 91-101.

Wang, Y.-C., and Ferguson, E. L. (2005). Spatial bistability of Dpp-receptor interactions during Drosophila dorsal-ventral patterning. Nature *434*, 229-234.